World Electric Vehicle Journal

MDPI

Article

Design of Permanent Magnet-Assisted Synchronous Reluctance Motor with Low Torque Ripple

Xinmin Li [1], Zihan Sun [1], Wenbo Sun [2], Liyan Guo [1,*] and Huimin Wang [1]

[1] School of Electrical Engineering, Tiangong University, Tianjin 300387, China
[2] WEICHAI Power Co., Ltd., Weifang 261061, China
* Correspondence: guoliyan@tju.edu.cn; Tel.: +86-150-0221-9635

Abstract: Permanent magnet-assisted synchronous reluctance motors (PMSRMs) have been widely used in household appliances, national defense and the military, due to their advantages of low cost and high efficiency. However, their excessive torque ripple cause a series of problems, such as high vibration and noise. To solve this problem, this paper first considers the important factor that causes the torque ripple—the cogging torque. Firstly, the generating principle of the cogging torque is analyzed, and a method combining magnetic pole migration and the stator auxiliary groove is proposed. On this basis, considering the position, width, depth, quantity and shape of the auxiliary groove, the Taguchi method is used to optimize the proposed improved structure. Finally, a new motor structure that can minimize torque ripple is obtained. Compared with the original structure, the cogging torque is reduced by 57.6%, the torque ripple is reduced by 38%, and the electromagnetic torque is only reduced by 1.6%.

Keywords: permanent magnet-assisted synchronous reluctance motors (PMSRMs); low torque ripple; low cogging torque; permanent magnet shifting; stator auxiliary groove; Taguchi method

Citation: Li, X.; Sun, Z.; Sun, W.; Guo, L.; Wang, H. Design of Permanent Magnet-Assisted Synchronous Reluctance Motor with Low Torque Ripple. *World Electr. Veh. J.* **2023**, *14*, 82. https://doi.org/10.3390/wevj14040082

Academic Editor: Joeri Van Mierlo

Received: 21 February 2023
Revised: 6 March 2023
Accepted: 21 March 2023
Published: 24 March 2023

1. Introduction

PMSRMs are widely used in household appliances [1], electric vehicles [2], aerospace [3] and other fields due to their significant advantages of small size, low loss and high efficiency. However, excessive torque ripple seriously affects the stability of motor operation. It then causes a series of problems, such as high vibration, high noise and a short lifespan. Therefore, reducing torque ripple is very important for the performance of the motor.

The torque ripple is mainly caused by ripple torque and cogging torque. No matter what operating conditions the motor is in, cogging torque will cause torque ripple. Therefore, cogging torque is an important factor of torque ripple. Cogging torque is produced by the tangential force that interacts with the permanent magnet and the stator cogging in order to maintain alignment. Its basic period number is equal to the least common multiple of the number of poles and slots in the motor [4]. A periodic cogging torque can be regarded as the superposition of harmonics after the Fourier decomposition. Therefore, reducing cogging torque can be started by reducing each harmonic amplitude of cogging torque. On the one hand, in order to reduce the amplitudes of some of the sub-harmonics of cogging torque, the amplitudes of the superposed harmonics of cogging torque can be changed by the relative offset of some sub-slot torque harmonics. Then, some subharmonics are completely eliminated under the appropriate offset angle. At present, the structural migration of the stator or pole can be divided into two types: axial migration and circumferential migration. In terms of axial migration, the literature [5] proposes a multistage stator tilt structure for the transverse flux motor, which reduces the cogging torque by 96%. However, this is not suitable for an ordinary interior permanent magnet synchronous motor. The literature [6] proposes three piecewise skew pole modes to achieve axial migration. The optimal offset mode was selected by finite element simulation, which reduced the

cogging torque by about 80%. However, the corresponding relation between the offset angle and the cogging torque is not given in the literature. In terms of circumferential migration, the literature [7] proposes a magnetic pole migration method for the interior permanent magnet synchronous motor. Based on the Taguchi method, the magnetic pole offset angle and permanent magnet size are comprehensively optimized, which greatly reduces the cogging torque. However, the corresponding relation between the magnetic pole migration and the slot torque is also not given in the literature. The literature [8] deduces the corresponding relationship between the magnetic pole offset angle and the cogging torque, and has proposed three offset modes. The most effective way to reduce the cogging torque is optimized.

On the other hand, the harmonic amplitudes of the cogging torque can be reduced by changing the magnetic circuit structure. The literature [9] reduces the harmonic content of the radial component of the magnetic density of the air gap by changing the eccentricity of the eccentric magnetic pole. As such, the cogging torque is reduced. However, this method is only applicable to a surface-attached motor and has some limitations. The literature [10] proposes a cross-shaped magnetic barrier structure for a synchronous reluctance motor in order to reduce the harmonic content of the magnetic density of the air gap. Then, the optimal magnetic barrier structure size used to reduce torque ripple is obtained by using the equivalent magnetic circuit method. However, the derivation process is relatively complicated. In order to reduce the volume of the air gap, the literature [11] proposes three shapes of auxiliary convex grooves to be used in the stator teeth. The simulation shows that the semi-circular shape has the best effect, and can reduce the cogging torque by 90%. However, only the shape of the auxiliary convex grooves is considered in this literature. The literature [12] increases the number of cycles of the cogging torque by opening auxiliary grooves in the stator teeth, thus reducing the cogging torque by 38%. However, only the shape and number of the auxiliary grooves are considered.

In order to reduce the amplitude of each harmonic wave of the slot torque, the relative offset of a harmonic wave of the slot torque and the change in the magnetic circuit structure are considered. A method combining magnetic pole migration and the stator auxiliary slot is proposed. In addition, in order to determine the position, width, depth, quantity and shape of the auxiliary slots, the proposed improved structure needs to be optimized.

In the optimization design of the motor parameters, not only the mutual influence of several optimization variables need to be considered, but also the different performances of the motor need to be taken into account. To solve this problem, a multi-objective optimization design method should be adopted. At present, the commonly used multi-objective optimization design methods mainly include genetic algorithm [13], differential evolution algorithm [14] and particle swarm optimization algorithm [15]. However, the above intelligent optimization algorithms have seevral problems, such as complex solution processes and long solution times. Correspondingly, the Taguchi method, established by Dr. Genichi Taguchi in Japan, is a low-cost and cost-effective multi-objective optimization design method. This method can greatly reduce the number of tests, reduce test costs and improve design efficiency, and is widely used in the field of motor design [16,17]. In the literature [18], the Taguchi method has been used to optimize the parameters of a reluctance motor, so that the no-load back electric of the motor is closer to sine and the cogging torque is lower. Similarly, the Taguchi method is adopted in the literature [19] in order to optimize the position of permanent magnets and improve the average torque, torque ripple and efficiency of the motor. The literature [20] also optimizes the stator structure of the motor using the Taguchi method in order to improve the working efficiency of the motor. Therefore, the Taguchi method is adopted in this paper to match the five key factors so as to minimize the torque ripple: the position, width, depth, quantity and shape of the auxiliary groove.

In order to reduce the torque ripple of PMSRM, a method combining pole migration and the stator auxiliary slot is proposed based on the cogging torque, which causes the torque ripple. The method mainly reduces the cogging torque by reducing the amplitude

of each harmonic wave. This paper first introduces the structure and he basic parameters of the motor, and analyzes the cogging torque generation and the reduction principle. On this basis, a new structure that combines magnetic pole migration and the stator auxiliary groove is proposed. The Taguchi method is used to match the five key factors of the position, width, depth, quantity and shape of the auxiliary slot. Finally, a new motor structure that can minimize torque ripples is obtained.

2. Theoretical Analysis of Motor Structure and Cogging Torque

This section firstly introduces the original structure and basic parameters of the permanent magnet-assisted synchronous reluctance motor. Then, the generating principle of cogging torque is analyzed. Finally, the principle of reducing cogging torque using magnetic pole migration and the principle of reducing cogging torque using the stator tooth opening auxiliary slot are analyzed.

2.1. Motor Structure and Basic Parameters

In this study, a 4-pole 36-slot PMSRM was taken as the research object. The structure of the original motor is shown in Figure 1, and the stator windings are distributed at short-distance windings. The basic parameters of the motor are shown in Table 1.

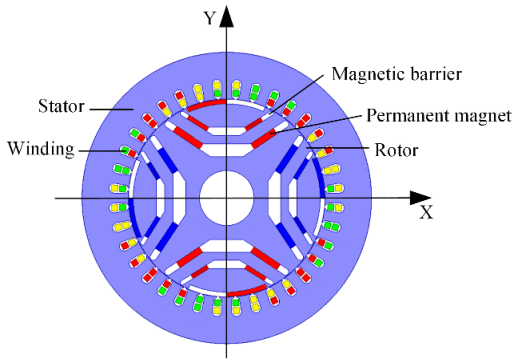

Figure 1. Original motor structure.

Table 1. Motor specific parameters.

Parameters	Symbol	Value	Unit
Rated speed	n_N	3000	r/min
Rated current	I_N	42	A
Number of pole Pairs	p	2	-
Number of slots	z	36	-
Radius of the stator inner surface	R_1	90.1	mm
Radius of rotor outer surface	R_2	89.6	mm
Radius of the stator outer surface	R_s	132.6	mm
Length of motor	l_s	155	mm

2.2. Cogging Torque Generation Principle

In order to more easily describe the mathematical model of PMSRM, without affecting the electromagnetic performance analysis of the motor, the following assumptions are made, assuming that the three-phase winding in the stator groove is evenly distributed. At the same time, it is assumed that the three-phase alternating current added by the stator windings is the standard sinusoidal alternating current. It is assumed that the various losses generated inside the permanent magnet are small and the permeability of the motor core is infinite and can be omitted. Since the magnetic permeability of the motor core is

infinite, the total energy W in the motor can be regarded as the sum of the magnetic field energy of the permanent magnet and air gap. The expression is as follows [21]:

$$W = W_{\mathrm{PM}} + W_{\mathrm{air}} = \frac{1}{2\mu_0}\int_V B^2(\theta,\alpha)\mathrm{d}V \tag{1}$$

where μ_0 is the vacuum permeability and V is the air gap volume. The expression of the air gap magnetic density $B(\theta,\alpha)$ is as follows:

$$B(\theta,\alpha) = B_{\mathrm{r}}(\theta)G(\theta,\alpha) \tag{2}$$

where $B_{\mathrm{r}}(\theta)$ is the circumferential distribution of the remanent magnetic field of the permanent magnet; $G(\theta,\alpha)$ is the circumferential distribution of the effective air gap's relative permeability; θ is the electrical angle of the rotor; and α is the relative position angle between the fixed rotors.

Cogging torque is the negative derivative of energy W with respect to the relative position angle α between fixed rotors when the motor is unloaded, as shown in the following formula:

$$T_{\mathrm{c}}(\alpha) = -\frac{\partial W}{\partial \alpha} \tag{3}$$

After substituting Equations (1) and (2) into Equation (3), the Fourier expansion of cogging torque can be obtained as follows:

$$T_{\mathrm{c}}(\alpha) = \frac{\pi z l_{\mathrm{s}}}{4\mu_0}(R_1^2 - R_2^2)\sum_{n=1}^{\infty} nG_n B_{\mathrm{r}(nz/2p)} \sin nz\alpha \tag{4}$$

where z is the number of stator slots; l_{s} is the axial length; R_1 is the inner radius of the stator; R_2 is the outer radius of the rotor; n is the harmonic frequency of the air gap flux density and can make $nz/2p$ an integer; and G_n is the permeability of the motor to the n order of the air gap flux density. The specific expression of $B_{\mathrm{r}(nz/2p)}$ is as follows:

$$B_{\mathrm{r}(nz/2p)} = \frac{4p}{nz\pi}B_{\mathrm{r}}^2 \sin(\frac{nz}{2p}\alpha_p\pi) \tag{5}$$

where p is the number of magnetic poles, and α_p is the polar arc coefficient.

As can be seen from Equation (4), the total cogging torque can be seen as the superposition of various harmonics, and reducing the amplitude of each harmonic of the cogging torque can effectively reduce the cogging torque.

2.3. Cogging Torque Reduction Principle

2.3.1. Magnetic Pole Migration Principle

It can be seen from Equation (4) that the total cogging torque can be seen as the superposition of harmonics. Similarly, the cogging torque generated by a single magnetic pole can also be seen as the superposition of harmonics. Since each harmonic of the cogging torque is periodic, it can be expressed as a vector form. In addition, because the rotor pole of the traditional permanent magnet motor is arranged symmetrically, the total cogging torque is in the phase superposition of the cogging torque that is generated by each magnetic pole. For example, T_{cog} of the total cogging torque fundamental, which is generated by two symmetrically arranged magnetic poles, is T_{cog1} of the cogging torque fundamental of magnetic pole 1, and is T_{cog2} of the cogging torque fundamental of magnetic pole 2 in phase superposition, as shown in Formula (6).

$$\begin{aligned} T_{\mathrm{cog}} &= T_{\mathrm{cog1}} + T_{\mathrm{cog2}} \\ &= 1\angle 0^\circ + 1\angle 0^\circ \\ &= 2\angle 0^\circ \end{aligned} \tag{6}$$

When magnetic pole 2 is offset 90° from magnetic pole 1, the base wave amplitude of the superimposed cogging torque will be reduced, as shown in Formula (7).

$$\begin{aligned} T_{\text{cog}} &= T_{\text{cog1}} + T_{\text{cog2}} \\ &= 1\angle 0^\circ + 1\angle 90^\circ \\ &= \sqrt{2}\angle 45^\circ \end{aligned} \tag{7}$$

When magnetic pole 2 is offset 180° from magnetic pole 1, the phenomenon of peak-valley elimination will occur, even if the fundamental wave of cogging torque after superposition completely disappears, as shown in Formula (8).

$$\begin{aligned} T_{\text{cog}} &= T_{\text{cog1}} + T_{\text{cog2}} \\ &= 1\angle 0^\circ + 1\angle 180^\circ \\ &= 0 \end{aligned} \tag{8}$$

Therefore, the appropriate angle of the magnetic pole relative offset will cause some harmonics of the cogging torque to produce a peaking and valley effect, thus reducing the cogging torque. The single magnetic pole migration formula of the nth harmonic of the cogging torque is as follows [8]:

$$\theta_n = \frac{\pi}{nN_{2pz}} \tag{9}$$

where N_{2pz} is the least common multiple of the number of poles and slots of the motor.

2.3.2. Principle of Stator Auxiliary Slot

It can be seen from Equation (4) that cogging torque is related to all harmonic amplitudes and the gap volume of the air gap flux density. In order to take these two factors into consideration, the concavity of the stator auxiliary groove can be changed. On the one hand, the base amplitude of the air gap flux density can be reduced by opening auxiliary grooves in the stator teeth. Because the period number of cogging torque is equal to the minimum common multiple of the number of poles and slots of the motor, the auxiliary groove is opened to increase the number of slots z, which can make the period number of cogging torque increase, so as to reduce the cogging torque and torque ripple. On the other hand, opening auxiliary convex slots in the stator teeth can reduce the volume of the air gap, but also increase the amplitude of the magnetic density of the air gap. Therefore, simulation can be used to find a suitable convex slot size to achieve cogging torque and reduce torque ripples. In addition, in order to comprehensively consider the influence of the various factors of the auxiliary groove on torque ripple, the Taguchi method will be adopted to determine the specific dimensions of each key factor of the auxiliary groove.

3. Motor Structure Design

In this section, a new magnetic pole migration structure is proposed based on the principle of reducing cogging torque with magnetic pole migration. Since the asymmetrical pole migration structure can produce a large and unbalanced magnetic pull, and a low and unbalanced magnetic pull, a low cogging torque and low torque ripple after pole migration are used as optimization objectives in order to select an optimal pole migration structure. In order to further reduce the cogging torque and torque ripple, this section opens an auxiliary slot on the stator tooth on the basis of the magnetic pole offset structure, and uses the Taguchi method to match the five key factors of the position, width, depth, number and shape of the auxiliary slot. The optimization goal is to minimize the torque ripple and maximize the electromagnetic torque, so as to minimize the torque ripple while maintaining the original electromagnetic torque.

3.1. Magnetic Pole Migration Structure Design

In order to describe the magnetic poles more clearly, the four magnetic poles in the motor are named 1–4 respectively at first, as shown in Figure 2a. Then, the two mag-

netic poles are regarded as a group of peak and valley elimination effects, that is, one of the magnetic poles is fixed, and the other magnetic pole is rotated counterclockwise on the basis of the symmetrical arrangement of the original magnetic pole in order to create harmonics cogging torque, and thus achieve the peak and valley elimination effect. For a 4-pole 36-slot motor, the number of poles and slots in the motor is put into Equation (9). It can be found that in order to weaken the fundamental harmonic T_{c1} of cogging torque, a single magnetic pole should be offset at 5°, as shown in Figure 2b. In order to weaken the second harmonic T_{c2} of cogging torque, the relative deviation angle of a single magnetic pole is 2.5°. In addition, in order to determine the direction of magnetic pole offset, in addition to the known magnetic pole offset angle, it is necessary to determine which magnetic poles are offset on the basis of the original symmetry. For the 4-pole 36-slot motor, the total cogging torque is the cogging torque generated by four magnetic poles in the same phase superposition; here, two magnetic poles are considered as a group of peak and valley elimination factors, which can be divided into two groups. Therefore, it is necessary to rotate both magnetic poles counterclockwise at the same time. At once, any two of the four magnetic poles are rotated, applying any of the 12 rotation modes; this involves, namely, rotating magnetic poles 12, 13, 14, 23, 24, 34, 21, 31, 41, 32, 42, 43. Because the order of the poles in each rotation does not affect the effect achieved, there are 6 rotation modes, namely 12, 13, 14, 23, 24, and 34. Among them, fixed magnetic pole 1 and 4, and rotating magnetic pole 2 and 3 have the same effect as fixed magnetic pole 2 and 3, and rotating magnetic pole 1 and 4; fixed pole 1 and 3 and rotating pole 2 and 4 have the same effect as fixed pole 2 and 4 and rotating pole 1 and 3; fixed magnetic pole 1 and 2 and rotating magnetic pole 3 and 4 have the same effect as fixed magnetic pole 3 and 4 and rotating magnetic pole 1 and 2. Therefore, after removing the repetitive mode, there are three rotation modes: mode 1: rotating magnetic pole 2 and 3 counterclockwise; mode 2: rotating magnetic pole 2 and 4 counterclockwise; and mode 3: rotating magnetic pole 3 and 4 counterclockwise. In addition, for the sake of expression, the original symmetric magnetic pole structure is named mode 0 here.

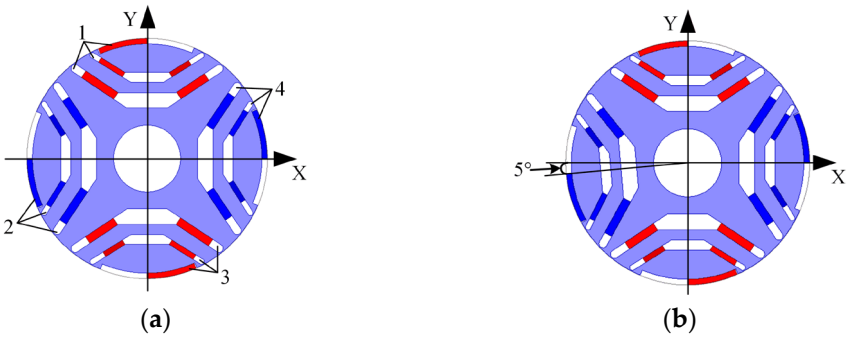

Figure 2. Magnetic pole diagram. (**a**) Magnetic pole nomenclature. (**b**) Single magnetic pole offset.

Firstly, the three magnetic poles are shifted 2.5° counterclockwise, respectively, and an optimal magnetic pole shift mode is selected. Then, the magnetic poles in this way are offset by 2.5° and 5° counterclockwise, respectively, in order to determine the final offset angle.

In addition to the cogging torque and torque ripples after pole migration, unbalanced magnetic pull should also be considered because asymmetric pole migration can produce a large imbalanced magnetic pull. The finite element simulation software "AYSYS Maxwell 19.2" was used to simulate the three magnetic pole migration modes, respectively, with a counterclockwise migration of 2.5°. In addition, the simulation calculation is carried out on the cogging torque T_c, cogging torque fundamental harmonic T_{c1}, cogging torque second harmonic T_{c2}, electromagnetic torque T, torque ripple T_r and the unbalanced magnetic tension F of the motor under no-load and rated load conditions (phase current effective

value 42 A and current angle 45.9°). The specific waveform comparison of each performance is shown in Figure 3. The specific values of each performance are shown in Table 2.

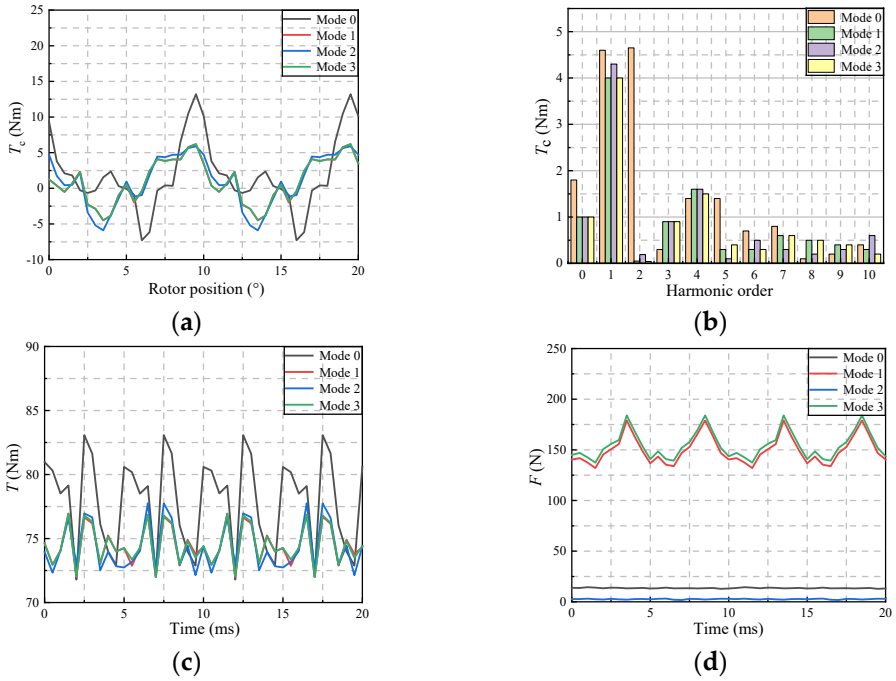

Figure 3. Performance comparison diagram of each mode. (**a**) Cogging torque waveform. (**b**) Cogging torque harmonic distribution. (**c**) Electromagnetic torque waveform. (**d**) Unbalance magnetic tension waveform.

Table 2. Performance comparison table of each mode.

Performance \ Mode	0	1	2	3
T_c (Nm)	13.2	6.2	5.9	6.2
T_{c1} (Nm)	4.6	4	4.3	4
T_{c2} (Nm)	4.65	0.05	0.19	0.04
T (Nm)	77.6	74.5	74.34	74.54
T_r (%)	8.9	5.8	6.4	5.7
F (N)	14	179	3	184

As can be seen from Figure 3 and Table 2, relative to the original structure (mode 0), modes 1–3 can effectively reduce the second harmonic of cogging torque and ensure torque reduction within 5%. However, the offset modes 1 and 3 both cause the imbalanced magnetic tension to rise significantly. This is mainly because the asymmetry of magnetic pole migration in modes 1 and 3 will make the resultant force on the rotor non-zero. That is, the magnetic pull generated by magnetic pole 1 and 3, magnetic pole 2 and magnetic pole 4 are asymmetrical and cannot cancel each other out. However, the magnetic pole migration mode of mode 2 has symmetry, which can still make the magnetic pull generated by magnetic pole 1 and 3, and magnetic pole 2 and 4 symmetrical and thus cancel each other. Therefore, the final mode of magnetic pole migration is mode 2; in this mode, magnetic pole 2 and 4 are offset, so as to reduce the torque ripple without worsening the unbalanced magnetic tension.

In addition, the offset angle of mode 2 needs to be determined, and the counterclockwise offset of mode 2 is 2.5° and 5°, respectively. The comparison of the performance waveforms at different angles is shown in Figure 4, and the specific values of each performance are shown in Table 3.

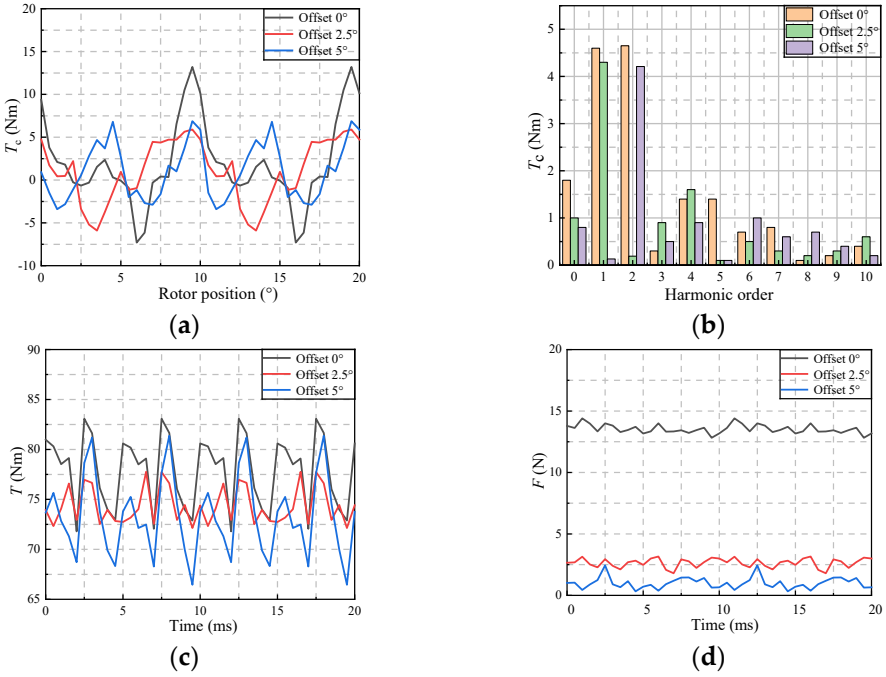

Figure 4. Performance comparison diagram from different angles. (**a**) Cogging torque waveform. (**b**) Cogging torque harmonic distribution. (**c**) Electromagnetic torque waveform. (**d**) Unbalance magnetic tension waveform.

Table 3. Performance comparison table at various angles.

Performance \ Offset Angle	0°	2.5°	5°
T_c (Nm)	13.2	5.9	6.87
T_{c1} (Nm)	4.6	4.3	0.13
T_{c2} (Nm)	4.65	0.19	4.21
T (Nm)	77.6	74.34	73.32
T_r (%)	8.9	6.4	12.4
F (N)	14	3	2.4

As can be seen from Figure 4 and Table 3, compared with the original structure (offset 0°), the second harmonic of cogging torque can be effectively weakened with an offset of 2.5°. Similarly, the fundamental harmonic of cogging torque can be effectively weakened with an offset of 5°, and the unbalanced magnetic tension of both methods does not increase. However, when the torque is offset by 5°, the torque decreases too much and the torque ripple increases. This is mainly because the available angle space between the magnetic poles is only 8.5°, and the distance between the magnetic poles is only 3.5° after the magnetic pole is offset by 5°. This will produce a large amount of magnetic leakage, thus reducing the output torque and increasing the torque ripple. In addition, since the primary and second harmonic amplitudes of the motor cogging torque are not much different, it is better to choose a pole offset of 2.5° in order to reduce the cogging torque. Thus, the final configuration of the offset poles is that poles 2 and 4 are offset by 2.5° counterclockwise. Compared with the original structure, the cogging torque was reduced by 55.3%, torque ripple was reduced by 28% and torque was reduced by 4.2%, which is less than 5% and within the allowable range. When auxiliary slots are opened for stator teeth later, the maximum torque is set as the optimization objective in order to achieve the increase in torque.

3.2. Stator Auxiliary Groove Design

In order to comprehensively consider the effects of the pole offset structure and the stator auxiliary slot structure on cogging torque, torque ripple and torque, this section introduces the auxiliary slot on the stator teeth based on the pole offset structure. The Taguchi method was used to analyze the influence of each optimization variable on torque and torque ripple, and the relative importance of the influence, so as to obtain the optimal size of each optimization variable in the auxiliary groove.

3.2.1. Optimize the Selection of Variables

In order to determine the position and shape of the auxiliary groove, at least 5 optimization variables are required, as shown in Figure 5. They are optimization variable *A*: the central angle corresponding to the bottom width of the auxiliary groove; optimization variable *B*: the depth of the auxiliary slot; optimization variable *C*: the number of auxiliary slots; optimization variable *D*: the shape of the auxiliary slot; and optimization variable *E*: the central angle corresponding to the space between the auxiliary slots.

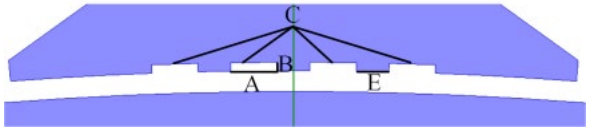

Figure 5. Schematic diagram of optimization variables.

Combined with the structural parameters of the motor, the value range of the above five optimization variables was determined. According to the original structure of the motor, the central angle corresponding to the notch is 1.4°, and the minimum value of the optimization variable *A* is 0°. In order to ensure the symmetry, the maximum value of optimization variable *A* is the central angle corresponding to the 1.4° notch, that is, the value range of variable *A* is 0°~1.4°. In order to comprehensively consider the concavity of the auxiliary groove, the positive value of variable *B* is specified to represent the auxiliary convex groove, and the negative value is specified to represent the auxiliary concave groove. Combined with the air gap length of 0.5 mm, the value range of variable *B* is determined to be −0.2 mm~0.2 mm. In order to ensure that the maximum bottom width of the auxiliary slots does not exceed the stator teeth, the central angle corresponding to the stator tooth width is 8.6° and the limitation of variable *A* is integrated. Variable *C* is taken as 1~4. In order to ensure the symmetry of the auxiliary slots, the general position of each auxiliary slot is determined according to the different values of variable *C*; if *C* is 1, the auxiliary slots are located on the center line of the stator teeth. If *C* is 2, the two auxiliary slots are located on the left and right sides of the center line of the stator teeth and are symmetric. If *C* is 3, the three auxiliary slots are located on the center line of the stator teeth, with the ones on the left and right side being symmetric. If *C* is 4, the positions of the four auxiliary slots are symmetrical and there are two on each side of the center line of the stator teeth. Optimization variable *D* considers the rectangle, triangle, arc and trapezoid, wherein the length of the rectangle, triangle base, arc string and trapezoid bottom are all determined by optimization variable *A*; meanwhile, the width of the rectangle, triangle height, arc depth and trapezoid height are all determined by optimization variable *B*. In addition, for the trapezoid, its upper base is taken as half of the lower base. In order to ensure that the maximum bottom width and the maximum interval of the auxiliary groove do not exceed the stator teeth, the optimization variable *E* should be selected according to the central angle corresponding to the stator tooth width, using optimization variables *A* and *C*. Due to the limitations of using the central angle corresponding to the stator tooth width and variables *A* and *C*, a unified variable *E* cannot be obtained. Therefore, the corresponding variable *E* intervals are set for different *C* variables, as shown in Table 4. The value range of variable *E* is from a to d.

Table 4. Different number of interval tables.

Number \ Interval	a	b	c	d
1	0°	0°	0°	0°
2	1°	2°	3°	4°
3	0.5°	1°	1.5°	2°
4	0.25°	0.5°	0.75°	1°

Four level values are evenly selected according to the value range of optimization variables *A*, *B* and *C*, and a factor level Table is established, as shown in Table 5.

Table 5. Factor level.

Level \ Factor	*A* (°)	*B* (mm)	*C*	*D*	*E*
1	0.35	−0.2	1	Rectangle	a
2	0.7	−0.1	2	Triangle	b
3	1.05	0.1	3	Arc	c
4	1.4	0.2	4	Trapezoid	d

According to the factor level Table, the corresponding orthogonal Table $L_{16}(4^5)$ is established, as shown in Table 6.

Table 6. $L_{16}(4^5)$ Orthogonal table.

Test Time	*A*	*B*	*C*	*D*	*E*
1	1	1	1	1	1
2	1	2	2	2	2
3	1	3	3	3	3
4	1	4	4	4	4
5	2	1	2	3	4
6	2	2	1	4	3
7	2	3	4	1	2
8	2	4	3	2	1
9	3	1	3	4	2
10	3	2	4	3	1
11	3	3	1	2	4
12	3	4	2	1	3
13	4	1	4	2	3
14	4	2	3	1	4
15	4	3	2	4	1
16	4	4	1	3	2

3.2.2. Test Results

The finite element simulation software "ANSYS Maxwell 19.2" was used to simulate 16 groups of orthogonal tests. Because the ultimate purpose of reducing cogging torque is to reduce torque ripple, in order to obtain the reduction effect of torque ripple more intuitively, the electromagnetic torque average value T and torque ripple T_r, which correspond to the 16 groups of orthogonal tests, are here analyzed. The specific calculation results are shown in Table 7.

Table 7. Test results.

Test Time	T (Nm)	T_r (%)
1	74.46	6.5
2	75.74	7.8
3	74.14	7.56
4	73.92	7.36
5	76.34	8.6
6	76.16	7.32
7	74.88	6.54
8	75.36	7.6
9	76.7	7.27
10	76.23	5.57
11	74.02	7.8
12	75.64	6.5
13	76.64	7.3
14	76.88	5.7
15	75.34	5.47
16	75.48	6.9

3.2.3. Results Processing

In order to analyze the influence of each optimization variable on the mean value T of electromagnetic torque and the torque ripple T_r, and their relative importance, it is necessary to carry out a mean value analysis and variance analysis on the results of the 16 groups of orthogonal tests.

1. Mean analysis

(1). Population mean analysis

Firstly, the overall mean value m of each column in Table 7 is obtained, and its calculation formula is as follows:

$$m = \frac{\sum_{i=1}^{n} m_i}{n} \tag{10}$$

In the formula, m_i is the test result of the i test in a column in Table 7, and n is the number of tests.

Equation (10) can be used to obtain the overall mean value of each column in Table 7. The calculation process of the overall mean value m_T of the mean value of electromagnetic torque is shown in Equation (11).

$$\begin{aligned} m_T &= \frac{T_1+T_2+\ldots+T_{16}}{16} \\ &= \frac{74.46+75.74+\ldots+75.48}{16} \\ &= 75.5 \end{aligned} \tag{11}$$

Similarly, the calculation process of m_{Tr} for the overall mean value of torque ripple is shown in Equation (12).

$$\begin{aligned} m_{Tr} &= \frac{T_{r1}+T_{r2}+\ldots+T_{r16}}{16} \\ &= \frac{6.5+7.8+\ldots+6.9}{16} \\ &= 5.68 \end{aligned} \tag{12}$$

(2). Average value analysis of all variables at all levels

Taking the mean value of electromagnetic torque T under each level of factor A as an example, the specific calculation process is as follows.

The solution process of $m_{TA(1)}$, which is the mean value of electromagnetic torque T under level 1 of factor A, is as follows:

$$\begin{aligned} m_{TA(1)} &= \frac{T_1+T_2+T_3+T_4}{4} \\ &= \frac{74.46+75.74+74.14+73.92}{4} \\ &= 74.57 \end{aligned} \tag{13}$$

Similarly, the mean value of electromagnetic torque T under level 2, 3 and 4 of factor A can be obtained. The solution process is as follows:

$$m_{TA(2)} = \frac{T_5 + T_6 + T_7 + T_8}{4} = 75.69 \tag{14}$$

$$m_{TA(3)} = \frac{T_9 + T_{10} + T_{11} + T_{12}}{4} = 75.65 \tag{15}$$

$$m_{TA(4)} = \frac{T_{13} + T_{14} + T_{15} + T_{16}}{4} = 76.1 \tag{16}$$

By the same token, the average value of electromagnetic torque and the torque ripple under various factors and levels can be obtained. The specific solving results are shown in Table 8.

Table 8. Average of factors at different levels.

Factor	Level	m_T (Nm)	m_{Tr} (%)
A	1	74.57	7.3
	2	75.69	7.5
	3	75.65	6.78
	4	76.1	6.3
B	1	76	7.4
	2	76.25	6.6
	3	74.6	6.8
	4	75.1	7.1
C	1	75	7.13
	2	75.76	7.09
	3	75.77	7.03
	4	75.4	6.7
D	1	75.46	6.3
	2	75.44	7.6
	3	75.55	7.16
	4	75.5	6.86
E	1	75.35	6.285
	2	75.7	7.13
	3	75.6	7.17
	4	75.3	7.365

As can be seen from Table 8, the combination of the horizontal values taken by the factors and that maximize the average electromagnetic torque is $A(4)B(2)C(3)D(3)E(2)$, and the combination of the horizontal values taken by the factors that minimize the torque ripple is $A(4)B(2)C(4)D(1)E(1)$. By observing these two combinations, it can be found that factor A and B can simultaneously make the different electromagnetic performances of the motor achieve the optimal value under the same level value. Therefore, factor A takes the common level value of 4 and factor B takes the common level value of 2. However, the factors C, D and E cannot make the different electromagnetic performances of the motor achieve the optimum at the same level. Therefore, it is necessary to use variance analysis to analyze the test results of the simulation of each group, in order to obtain the relative importance of each factor regarding different electromagnetic performances, and

then obtain the optimal combination of each factor level considering the electromagnetic torque and torque ripple.

2. Variance Analysis

In order to obtain the relative importance degree of each optimization variable's influence on the mean value of electromagnetic torque and torque ripple, it is necessary to conduct a variance analysis on the test results. The variance-solving process used for the mean value of the electromagnetic torque and torque ripple under each factor is as follows:

$$S_A = \frac{\sum_{j=1}^{Q} (m_{A(j)} - m)^2}{Q} \tag{17}$$

where S_A is the variance in an objective function under factor A; Q is the number of levels taken by each factor; $m_{A(j)}$ is the average value of an objective function under factor A level j; and m is the overall average value of the objective function.

Taking the variance of the average electromagnetic torque T under factor A as an example, the calculation process of this variance S_{TA} is as follows.

$$\begin{aligned} S_{TA} &= \tfrac{1}{4}\Big[\left(m_{TA(1)} - m_T\right)^2 + \left(m_{TA(2)} - m_T\right)^2 \\ &\quad + \left(m_{TA(3)} - m_T\right)^2 + \left(m_{TA(4)} - m_T\right)^2\Big] \\ &= \tfrac{1}{4}\Big[(74.57 - 75.5)^2 + (75.69 - 75.5)^2 \\ &\quad + (75.65 - 75.5)^2 + (76.1 - 75.5)^2\Big] \\ &= 0.32 \end{aligned} \tag{18}$$

Similarly, according to Equation (17), the average value of electromagnetic torque and the variance in torque ripple under various factors can be obtained, and the specific results of the solution are shown in Table 9.

Table 9. Variance under various factors.

Factor	S_T	S_{Tr}
A	0.32	0.22
B	0.45	0.1
C	0.1	0.02
D	0.001	0.22
E	0.03	0.17

In order to obtain the relative importance of each optimization variable on the average value of electromagnetic torque and torque ripple more intuitively, the proportion of variance under each factor is specified here. The formula for calculating the proportion of variance under each factor of the average value of torque is as follows:

$$K_{STx} = \frac{S_{Tx}}{S_{TA} + S_{TB} + S_{TC} + S_{TD} + S_{TE}} \times 100\% \tag{19}$$

where K_{STx} is the proportion of variance and S_{Tx} in the total variance.

Similarly, the formula for calculating the variance proportion of torque ripple under each factor is as follows:

$$K_{STrx} = \frac{S_{Trx}}{S_{TrA} + S_{TrB} + S_{TrC} + S_{TrD} + S_{TrE}} \times 100\% \tag{20}$$

where K_{STrx} is the proportion of variance and S_{Trx} in the total variance.

The specific results of the average value of electromagnetic torque and the proportion of variance in torque ripple under various factors are shown in Table 10.

Table 10. Variance under various factors.

Factor	K_{STx} (%)	K_{STrx} (%)
A	35.5	30.1
B	50	13.7
C	11.1	27.4
D	0.1	30.13
E	3.3	23.3

It can be seen from Table 10 that the impact of factors *C*, *D* and *E* on torque ripple is greater than that exerted on the average value of electromagnetic torque. Therefore, factors *C*, *D* and *E* are selected to minimize the torque ripple, that is, *C*(4), *D*(1) and *E*(1). Finally, the combination of the horizontal values of each factor is obtained as *A*(4)*B*(2)*C*(4)*D*(1)*E*(1), that is, the central angle corresponding to the bottom width of the stator auxiliary groove is 1.4°, the protrusion depth of the auxiliary groove is 0.1 mm, the number is 4, the shape of the auxiliary groove is rectangular, and the central angle corresponding to the interval between the auxiliary groove is 0.25°, as shown in Figure 6.

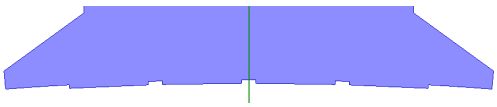

Figure 6. Stator tooth diagram.

In summary, the final motor structure is obtained, that is, the magnetic pole offset and the stator auxiliary slot structure. As shown in Figure 7, the structure effectively reduces the second harmonic of the cogging torque by shifting the magnetic poles 2 and 4 counterclockwise by 2.5°, and further reduces the harmonics of the cogging torque by adding auxiliary convex slots in the stator teeth.

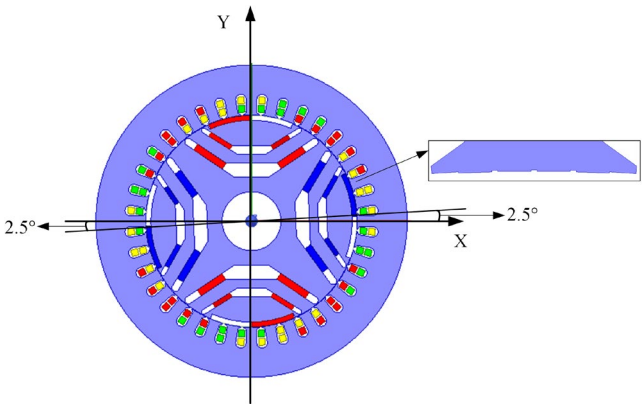

Figure 7. Final motor structure.

4. Motor Performance Analysis

In order to more intuitively show the superiority of the final motor structure (magnetic pole offset and stator auxiliary slot structure), the finite element simulation software "ANSYS Maxwell 19.2" is used to simulate the three different motor structures of the original structure, the offset magnetic pole structure, and the offset magnetic pole and stator auxiliary slot structure. The electromagnetic performance of the motor under no-load and rated load (the effective value of the phase current is 42 A, the current angle is 45.9°) is calculated. In order to facilitate the expression, the original structure is named model 0, the

offset magnetic pole structure is named model 1, and the offset magnetic pole and stator auxiliary slot structure is named model 2.

4.1. No-Load Performance Analysis

The cogging torque waveform comparison and harmonic comparison of each model are shown in Figure 8a,b, respectively. It can be found that compared with model 0, model 1 effectively reduces the second harmonic of the cogging torque due to the 2.5° counterclockwise shift in magnetic poles 2 and 4. Compared with model 1, model 2 effectively reduces the harmonics of the cogging torque due to the existence of the stator tooth auxiliary slot, which further reduces the cogging torque by 5.1%. At the same time, compared with model 0, model 2 reduces the cogging torque by 57.6%. Therefore, the structure has a better effect on reducing the torque ripple of the motor.

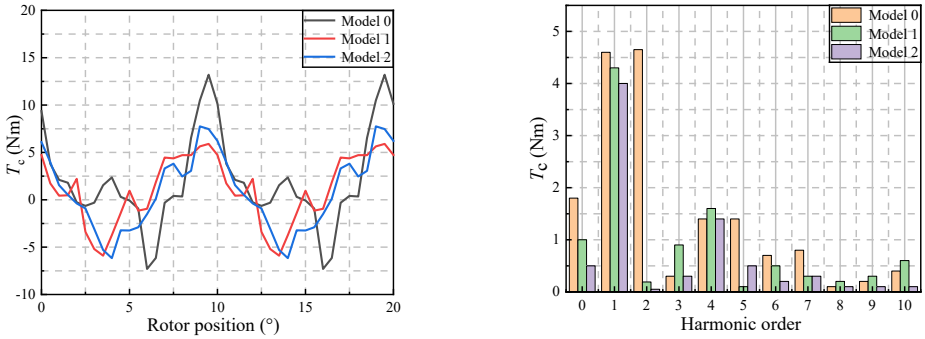

Figure 8. Cogging torque comparison diagram of each model. (**a**) Waveform contrast diagram. (**b**) Harmonic distribution diagram.

The comparison of the waveforms of the back electromotive force (EMF) and the flux linkage of each model A is shown in Figure 9a,b, respectively, and the specific numerical pairs are shown in Table 11. It can be found that their fundamental amplitude values have good consistency, which indicates that the electromagnetic torque provided by them is not very different. At the same time, their corresponding total harmonic distortion (THD) decreases in turn, which provides the possibility of reducing cogging torque and torque ripple.

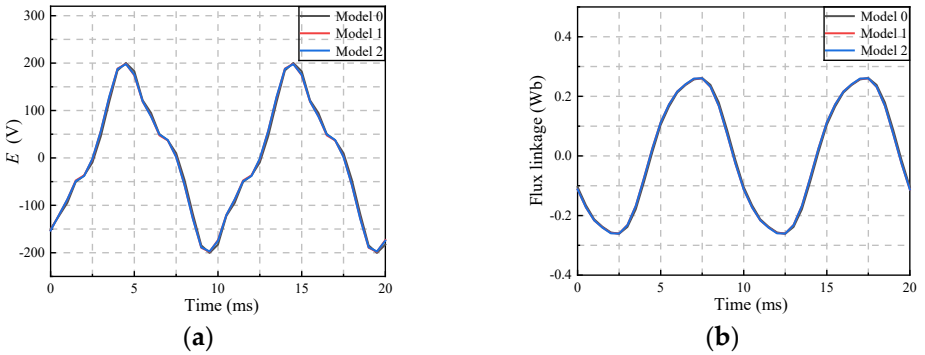

Figure 9. Comparison of A-phase performance of each model. (**a**) Back EMF waveform. (**b**) Flux linkage waveform.

Table 11. A-phase performance comparison table of each model.

Performance		Model 0	1	2
Back EMF	fundamental amplitude	170 V	169.6 V	169.9 V
	THD	22.03%	21.25%	20.96%
Flux linkage	fundamental amplitude	0.27 Wb	0.27 Wb	0.27 Wb
	THD	7.29%	7.26%	7.17%

4.2. On-Load Performance Analysis

The electromagnetic torque waveform comparison and specific numerical comparison of each model are shown in Figure 10 and Table 12, respectively. It can be seen that model 2 further reduces the torque ripple by 14% on the basis of model 1, and also increases the electromagnetic torque by 2.7%. Compared with model 0, model 2 reduces the torque ripple by 38% and the electromagnetic torque by only 1.6%, which proves the effectiveness of the proposed structure.

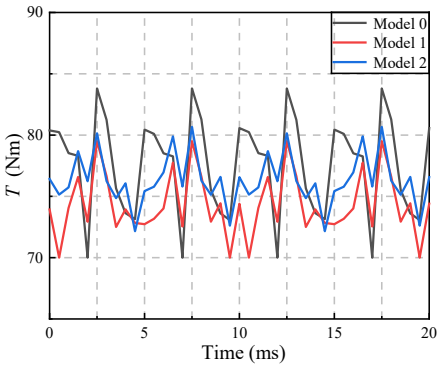

Figure 10. Comparison of electromagnetic torque of each model.

Table 12. Comparison table of electromagnetic torque of each model.

Performance	Model 0	1	2
Electromagnetic torque	77.6 Nm	74.34 Nm	76.32 Nm
Torque ripple	8.9%	6.4%	5.5%

In order to show the superiority of model 2 more comprehensively, the unbalanced magnetic pull of each model is also simulated. The specific waveform is shown in Figure 11a. It can be found that although the unbalanced magnetic pull of model 1 is the smallest, compared with model 0, model 2 does not deteriorate the electromagnetic performance of the unbalanced magnetic pull of the motor. Therefore, the unbalanced magnetic pull of model 2 is also within the allowable range. The core loss waveforms of each model are shown in Figure 11b. It is evident that the core losses of model 0, 1 and 2 are 351.38 W, 351.02 W and 363.15 W, respectively. Although the core loss provided by model 2 is the largest, it is only increased by 3.3% compared with model 0, which is less than 5%. Therefore, the core loss of the model is within the allowable range.

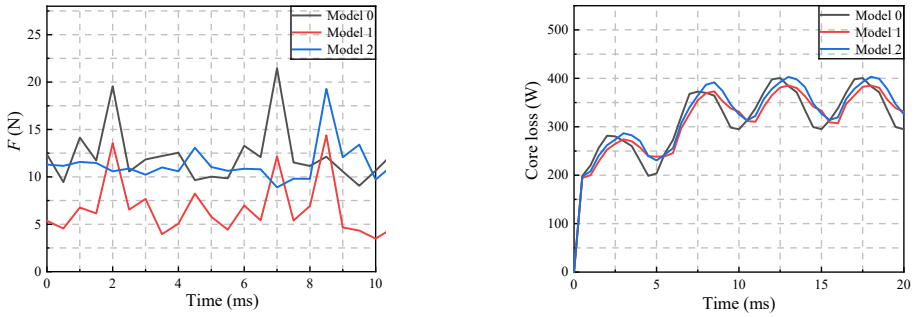

(**a**) (**b**)

Figure 11. Performance comparison diagram of each model. (**a**) Unbalance magnetic tension waveform. (**b**) Core loss comparison diagram.

5. Conclusions

In order to reduce the torque ripple of PMSRM, this paper starts with cogging torque, which is one of the main causes of torque ripple. By analyzing the generation and reduction principles involved in cogging torque, a new structure that combines pole offset and the stator auxiliary slot is proposed. In addition, the Taguchi method is used to comprehensively design the five key factors, which are the position, width, depth, number and shape of the auxiliary slot. Compared with the original structure, when the electromagnetic torque of the structure is reduced by only 1.6%, the cogging torque is reduced by 57.6%, and the torque ripple is reduced by 38%. At the same time, the electromagnetic properties of the structure do not deteriorate, so the effectiveness of the proposed structure is proven.

Author Contributions: Conceptualization, L.G. and X.L.; methodology, Z.S. and L.G.; software, Z.S.; formal analysis, Z.S. and L.G.; data curation, Z.S.; writing—original draft preparation, Z.S.; writing—review and editing, L.G., W.S., X.L. and H.W.; funding acquisition, L.G. and H.W. All authors have read and agreed to the published version of the manuscript.

Funding: This research was funded by the National Natural Science Foundation of China under Grant 52007132, and in part by the Program of Nuclear Power Technology Innovation Centre under Grant HDLCXZX-2021-ZH-015.

Data Availability Statement: The data presented in this study are available in the article.

Conflicts of Interest: W.S. is employee of WEICHAI Power Co., Ltd., Weifang 261061, China. The paper reflects the views of the scientists, and not the company.

References

1. Michele, D.; Mukhammed, M.; Wang, S.; Davide, B.; Giampaolo, B.; Werner, J.; Nicola, B.; Michael, G.; Chris, G. Optimised design of permanent magnet assisted synchronous reluctance machines for household appliances. *IEEE Trans. Energy Convers.* **2021**, *36*, 3084–3095.
2. Liu, X.P.; Li, Y.; Liu, Z.Q.; Ling, T.; Luo, Z.H. Analysis and design of a high power density permanent magnet-assisted synchronous reluctance machine with low-cost ferrite magnets for EVs/HEVs. *Compel.-Int. J. Compul. Math. Electr. Electron. Eng.* **2016**, *35*, 1949–1964. [CrossRef]
3. Guo, H.; He, X.; Xu, J.Q.; Tian, W.; Sun, G.Y.; Ju, L.C.; Li, D.H. Design of an aviation dual-three-phase high-power high-speed permanent magnet assisted synchronous reluctance starter-generator with antishort-circuit ability. *IEEE Trans. Power Electron.* **2022**, *37*, 12619–12635. [CrossRef]
4. Wang, X.H. *Permanent Magnet Motor*, 2nd ed.; China Electric Power Press: Beijing, China, 2011.
5. Ueda, Y.; Takahashi, H. Cogging torque reduction on transverse-flux motor with multilevel skew configuration of toothed cores. *IEEE Trans. Magn.* **2019**, *55*, 1–5. [CrossRef]
6. Jo, I.H.; Lee, H.W.; Jeong, G.; Ji, W.Y.; Park, C.B. A study on the reduction of cogging torque for the skew of a magnetic geared synchronous motor. *IEEE Trans. Magn.* **2019**, *55*, 1–5. [CrossRef]
7. Ruan, B.; Gu, A.Y.; Lian, Y.Z.; Hong, Z.C.; Liu, H.; Xu, Z.Y. Optimization design for torque ripple of IPMSM based on taguchi method and magnet shifting. *Micromotors* **2019**, *52*, 7–11.
8. Liu, G.H.; Du, X.X.; Zhao, W.X.; Chen, Q. Reduction of torque ripple in inset permanent magnet synchronous motor by magnets shifting. *IEEE Trans. Magn.* **2017**, *53*, 1–13. [CrossRef]

9. Zhou, Y.; Li, H.S.; Meng, G.W.; Zhou, S.; Cao, Q. Analytical calculation of magnetic field and cogging torque in surface-mounted permanent-magnet machines accounting for any eccentric rotor shape. *IEEE Trans. Ind. Electron.* **2015**, *62*, 3438–3447. [CrossRef]
10. Liang, J.; Dong, Y.; Sun, H.X.; Liu, R.Z.; Zhu, G.T. Flux-barrier design and torque performance analysis of synchronous reluctance motor with low torque ripple. *Appl. Sci.* **2022**, *12*, 3958. [CrossRef]
11. Herlina; Rudy, S.; Uno, B.S. Minimization of cogging torque based on different shape of anti-notch method. In Proceedings of the 2016 3rd International Conference on Information Technology, Computer, and Electrical Engineering (ICITACEE), Semarang, Indonesia, 19–20 October 2016; pp. 160–163.
12. Huang, Y.; Jiang, L.; Lei, H. Research on cogging torque of the permanent magnet canned motor in domestic heating system. *Energy Rep.* **2021**, *7*, 1379–1389. [CrossRef]
13. Fadranski, D.; Syré, A.M.; Grahle, A.; Göhlich, D. Analysis of charging infrastructure for private, battery electric passenger cars: Optimizing spatial distribution using a genetic algorithm. *World Electr. Veh. J.* **2023**, *14*, 26. [CrossRef]
14. Liu, Z.Y.; Hu, Y.; Wu, J.C.; Zhang, B.Y.; Feng, G.H. A novel modular permanent magnet-assisted synchronous reluctance motor. *IEEE Access* **2021**, *9*, 19947–19959. [CrossRef]
15. Liu, X.T.; Fan, X.J.; Wang, L.; Wu, J. State of charge estimation for power battery base on improved particle filter. *World Electr. Veh. J.* **2023**, *14*, 8. [CrossRef]
16. Yan, S.L.; Zhang, X.Y.; Gao, Z.D.; Wang, A.C.; Zhang, Y.F.; Xu, M.J.; Hua, S.Z. Design optimization of a new hybrid excitation drive motor for new energy vehicles. *World Electr. Veh. J.* **2023**, *14*, 4. [CrossRef]
17. Cheng, P.; Yang, X.J.; Lan, H.; Hong, Y.Y.; Dai, Q. Design and efficiency optimization of a synchronous generator using finite element method and taguchi method. *Electr. Mach. Control.* **2019**, *23*, 94–99+104.
18. Liu, Y.L.; Yu, H.T.; Wang, Y. Establishment of a new dual rotor flux switching motor magnetic circuit model and optimization of no-load back EMF. *IEEE Trans. Magn.* **2019**, *55*, 1–5. [CrossRef]
19. Xu, J.W.; Gao, L.Y.; Zeng, L.B.; Pei, R.L. Optimum design of interior permanent magnet synchronous motor using taguchi method. In Proceedings of the 2019 IEEE Transportation Electrification Conference and Expo (ITEC), Detroit, MI, USA, 19–21 June 2019; pp. 1–4.
20. Hwang, C.C.; Hung, S.S.; Liu, C.T.; Cheng, S.P. Optimal design of a high speed SPM motor for machine tool applications. *IEEE Trans. Magn.* **2014**, *50*, 1–4. [CrossRef]
21. Xu, M.J.; Zhang, X.Y.; Wang, J.; Yan, S.L.; Yin, H.B.; Zhou, Y.C. Cogging torque reduction method of internal permanent magnat motor based on stator tooth shoulder chamfer. *J. Hebei Univ. Sci. Technol.* **2021**, *42*, 561–569.